Progress towards practical device-independent quantum key distribution with spontaneous parametric down-conversion sources, on-off photodetectors, and entanglement swapping

Kaushik P. Seshadreesan, Masahiro Takeoka, and Masahide Sasaki

Phys. Rev. A **93**, 042328 — Published 18 April 2016

DOI: 10.1103/PhysRevA.93.042328

Towards practical device-independent quantum key distribution with spontaneous parametric downconversion sources, on-off photodetectors and entanglement swapping

Kaushik P. Seshadreesan,[1,2,3] Masahiro Takeoka,[1] and Masahide Sasaki[1]

[1]*National Institute of Information and Communications Technology, Koganei, Tokyo 184-8795, Japan*
[2]*Hearne Institute for Theoretical Physics and Department of Physics and Astronomy, Louisiana State University, Baton Rouge, Louisiana 70803, USA*
[3]*Max-Planck-Institut für die Physik des Lichts, Günther-Scharowsky-Straße 1, Bau 24, 91058 Erlangen, Germany*

Device-independent quantum key distribution (DIQKD) guarantees unconditional security of secret key without making assumptions about the internal workings of the devices used. It does so using the loophole-free violation of a Bell's inequality. The primary challenge in realizing DIQKD in practice is the detection loophole problem that is inherent to photonic tests of Bell's inequalities over lossy channels. We revisit the proposal of Curty and Moroder [Phys. Rev. A 84, 010304(R) (2011)] to use a linear optics-based entanglement-swapping relay (ESR) to counter this problem. We consider realistic models for the entanglement sources and photodetectors; more precisely, (a) polarization-entangled states based on pulsed spontaneous parametric downconversion (SPDC) sources with infinitely higher order multi-photon components and multimode spectral structure, and (b) on-off photodetectors with non-unit efficiencies and non-zero dark count probabilities. We show that the ESR-based scheme is robust against the above imperfections and enables positive key rates at distances much larger than what is possible otherwise.

I. INTRODUCTION

Quantum cryptography [1, 2] uses the laws of quantum mechanics to establish unconditional security of data transmission—meaning that the encrypted data can be secure against an eavesdropper of unbounded abilities. The BB84 [3] and a host of other protocols proposed since [4–8] guarantee such unconditional security in quantum key distribution (QKD) when the physical components used are well characterized and trustworthy. However, such ideal conditions cannot be met perfectly in the real world. The implementation of the physical devices may have imperfections more or less, i.e., side channels. Also, the components may have been manufactured by a malicious party, introducing backdoors into them. Real world quantum crypto-systems are hence amenable to a plethora of possible attacks through side channels and backdoors. This has stimulated great interest in a model for cryptography that establishes security independently of the internal workings of the physical devices used and is thus inherently immune to side-channel attacks and backdoors, provided that the given devices are operated in secure locations by the legitimate sender (Alice) and receiver (Bob) [9]. Such a "device independent" (DI) model for QKD has been carefully studied and its security proven under fairly general conditions (cf. [10–12] and references therein).

Unconditional security in DIQKD is typically guaranteed by means of the loophole-free violation of a Bell's inequality, where both the locality and the detection loopholes are closed simultaneously [13]. The first-ever loophole-free Bell test has been performed with electron spins in nitrogen vacancy (NV) centers in diamonds [14]. The first-ever all-optical loophole-free Bell tests [15, 16] have also been realized recently. Yet, photonic Bell tests over long-distance communication channels are bound to suffer from the detection loophole problem due to transmission and fiber-coupling losses. Nevertheless, there have been proposals to mitigate transmission losses using non-deterministic strategies. In particular, inspired by Ralph and Lund's idea for a non-deterministic photon amplifier [17], Gisin et al. [18] proposed a heralded qubit amplifier that utilizes quantum teleportation to boost the amplitude of the maximally entangled component of a lossy entangled state. The qubit amplifier was demonstrated experimentally by Kocsis et al. [19, 20]. It is, however, technically far from feasible for application in DIQKD. Curty and Moroder [21] investigated a conventional entanglement-swapping relay (ESR) node based on linear optics (Fig. 1). Rather than amplifying the maximally entangled compo-

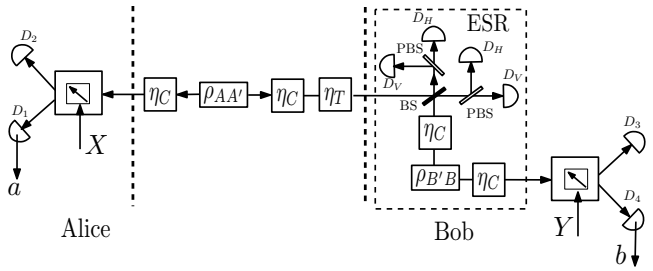

FIG. 1: Setup for DIQKD with a conventional entanglement-swapping relay (ESR) node based on linear optics. A source $\rho_{AA'}$ distributes polarization entanglement to receivers Alice and Bob. The distributed states are subject to losses in fiber coupling (both in the channel to Alice as well as to Bob) and transmission (in the channel to Bob, who is situated far from the source), the respective efficiencies being η_T and η_C. Bob employs a ESR node, which consists of another similar entanglement source $\rho_{BB'}$, beam splitters (BS: 50:50 beam splitter, PBS: Polarizing beam splitter) and heralding detectors D_H and D_V corresponding to horizontal and vertical polarizations. Upon each successful entanglement swapping event, Alice and Bob perform polarization measurement with polarizer settings X, Y, respectively, and the outcomes are denoted as a, $b \in \{+1, -1\}$, respectively. The detectors are assumed to be imperfect, on-off photodetectors, with non-unit efficiencies and non-zero dark-count probabilities.

nent in the lossy state, the relay node simply ensures that the state heralded upon successful entanglement swapping sufficiently violates the Clauser-Horne-Shimony-Holt (CHSH) inequality [22] in a loophole-free test. The authors showed that the relay node enables higher key rates than what is possible with the teleportation-based qubit amplifier when photon number resolving detectors (PNRD) are used and the product of coupling and detector efficiencies is higher than 95%. High efficiency entanglement swapping has been successfully demonstrated in numerous optical experiments [23–25]. More recently, in an alternative approach, DIQKD based on local Bell tests has been considered and its security investigated [26].

In this work, we revisit the scheme of Curty and Moroder based on entanglement swapping [21] with realistic models for the entanglement sources and detectors. We consider sources of polarization-entanglement, which are based on a pair of pulsed spontaneous parametric down conversions (SPDCs) with infinitely higher order multiphoton components and multimode spectral structure. Pulsed sources are preferred over continuous-wave sources in many practical applications, because they generate temporally localized signals which are more suitable for photon counters and coincidence count measurements. On the other hand, these signals are generated in spectrally multiple modes, which makes it more difficult to match the mode of interest between the devices used, especially when dispersive components are involved in the experimental setup. Thus, in order to improve the visibility of correlation measurements, careful multimode analysis is necessary. This is our motivation to include the multimode spectral structure of the sources in our model. We model our detectors as on-off photodetectors—detectors that merely distinguish the event of presence of photons from absence, and include losses and dark counts. The detector efficiencies are assumed to be flat over all the spectral modes. We show that the relay node enables positive key rates at distances larger than what is possible without the relay node for sufficiently large coupling and detector efficiencies, small dark count probabilities in the detectors and small spectral spread in the sources. Our analyses are non-perturbative and exact. They involve the use of tools from Gaussian quantum information that are based on characteristic functions.

The paper is organized as follows. In Section II, we recall the basics of DIQKD and outline the ESR-assisted scheme for DIQKD. In Section III, we describe our realistic model for the sources of polarization entanglement in the scheme, which includes their higher order multi-photon components and multimode spectral structure. In Section IV, we present our results. Section V captures our main conclusions.

II. DIQKD USING AN ENTANGLEMENT-SWAPPING RELAY

A. Basic principle of DIQKD

First of all, we recall the basic principle of DIQKD between two parties Alice and Bob [27]. A typical protocol for DIQKD involves: (a) a "black-box" source that transmits shares of an entangled quantum state to Alice and Bob through lossy communication channels, and (b) a blackbox measurement apparatus at each of Alice and Bob. The apparatus at Alice has three possible measurement

settings $X_i \in \{X_0, X_1, X_2\}$, while the one at Bob has two possible settings, namely $Y_j \in \{Y_1, Y_2\}$. All the measurement observables are taken to have binary outcomes, i.e., $a_i,\ b_j \in \{+1, -1\}$. For example, in an optical protocol for DIQKD based on polarization entanglement, the different measurement settings would correspond to different polarizer settings, and the outcomes to the clicking of one of two detectors placed in orthogonal polarization modes. The only assumption involved is that Alice and Bob are in secure locations such that no classical information either about the choice of measurement settings or the observed outcomes leaks out without their permission.

Alice and Bob perform repeated measurements under the setting $\{X_0, Y_1\}$ to generate the raw key. The qubit error rate (QBER) associated with the raw key is defined as $P(a \neq b | X_0 = Y_1)$. Over a subset of uses of the communication channel, Alice and Bob use the measurement settings $\{X_1, X_2\}$ and $\{Y_1, Y_2\}$ to test the CHSH functional

$$\mathcal{CHSH} = \langle a_1 b_1 \rangle + \langle a_1 b_2 \rangle + \langle a_2 b_1 \rangle - \langle a_2 b_2 \rangle , \quad (1)$$

where $\left\langle a_i b_j \right\rangle = P\left(a = b \middle| X_i Y_j\right) - P\left(a \neq b \middle| X_i Y_j\right)$. A value of $\mathcal{CHSH} > 2$ indicates the presence of nonlocal correlations in the state and is used to bound Eve's knowledge about the key. We denote the maximal possible value of $\mathcal{CHSH}$ for a given state with the corresponding sets of optimal measurement observables $\{X_1, X_2\}$ and $\{Y_1, Y_2\}$ by S. S can at best take the value $2\sqrt{2}$, known as the Cirelson bound [28], and is achieved by the maximally entangled state. The key rate is a function of S and the QBER. A conservative lower bound on the rate of generating key that is secure against the so-called collective eavesdropping attacks (i.e., where the attack is independent and identical during each use of the communication channel) is given by the Devetak-Winter formula [29]:

$$K \geq 1 - h(Q) - \chi(S) , \quad (2)$$

where K is the number of secret bits that can be generated per channel use, S is the maximal violation, Q is QBER,

$$\chi(S) = h\left(\frac{1 + \sqrt{(S/2)^2 - 1}}{2}\right), \quad (3)$$

and $h(x)$ is the binary entropy given by $h(x) = -x \log x - (1-x)\log(1-x)$. It can be shown that $S > 2$ is a necessary condition to realize a positive key rate.

A crucial requirement on the Bell test for DIQKD is that it is performed in a loophole-free manner. We recall a simple strategy that has been used to perform a loophole-free test of the CHSH inequality for the realistic scenario under consideration [21]. Let us say that the clicking of Detector D_1 at Alice corresponds to outcome $a = +1$ and D_2 to $a = -1$ and similarly, the clicking of D_3 at Bob to $b = +1$ and D_4 to $b = -1$. When neither or both detectors at Alice (D_1, D_2) click, or likewise at Bob (D_3, D_4), the outcome is obviously inconclusive at the respective party. The strategy is to deterministically assign a conclusive outcome upon such detection events. For example, when neither or both detectors at Alice click, the outcome can be assigned the value $a = -1$, and at Bob $b = -1$.

B. Entanglement-Swapping Relay-assisted DIQKD

Suppose that the source of entanglement is located near Alice, and Bob is situated at a distance from both Alice and the source. The losses in the communication channel to Alice are thus attributed to fiber coupling and detector inefficiencies. On the other hand, the channel to Bob in addition suffers from transmission losses. We denote the fiber-coupling efficiency, the detector efficiency, and the transmission efficiency by η_C, η_{det} (or η_{hdet} in the case of heralding detectors) and η_T, respectively. We refer to the product $\eta_C \eta_{\text{det}}$ as detection efficiency η_D (or η_{HD} in the case of the heralding modes), while on the other hand, by "overall" detection efficiency, we mean the product $\eta_D \eta_T$. The overall detection efficiencies at Alice and Bob are thus given by η_D and $\eta_D \eta_T$, respectively. Recent results by Caprara-Vivoli et al. [30] have shown that a loophole-free test of the CHSH inequality in (1) based on the deterministic strategy described above requires an overall detection efficiency, which is at least 2/3 to exhibit a value of $S > 2$. Assuming ideal fiber coupling and detectors at both parties (i.e., $\eta_D = 1$), this corresponds to a distance of 8.8km for the optical fiber communication channel to Bob ($\alpha = 0.2$dB/km attenuation). Since $S > 2$ is a necessary condition for a positive key rate, the scope for DIQKD thus

appears to be severely limited at first look. However, as mentioned before [18, 21], it is possible to mitigate the effects of transmission losses on distillable key rate using probabilistic strategies, thereby extending the possible distances for DIQKD.

Consider the ESR-assisted scheme shown in Fig 1, as considered in Ref. [21]. To first approximation, the state generated by the source $\rho_{AA'}$ is a maximally polarization entangled photon pair, with a photon directed towards each of Alice and Bob. Alice performs polarization measurement on her share of the state. Bob, on his part, employs an ESR node to the state received through the lossy channel. That is, he mixes the incoming state on a 50:50 beamsplitter with one share of another polarization entangled state $\rho_{B'B}$, which is similar to $\rho_{AA'}$ and performs polarization measurement on the output modes. When entanglement swapping succeeds, (i.e., when either of the pair of heralding detectors D_6 and D_7 or D_5 and D_8 placed in the output modes click and the respective other pair doesn't) Bob performs a polarization measurement on the other share of the entangled state $\rho_{B'B}$. The parties then apply the deterministic strategy of assigning conclusive values to inconclusive outcomes mentioned above to perform DIQKD based on the (loophole-free) CHSH test. Naturally, the key rate in the ESR-assisted scheme now includes a factor corresponding to the probability of success of the relay node. Although this success probability drops exponentially with growing distance, the distances over which positive key rate can be achieved with ideal fiber coupling and detectors still improves by an order of magnitude compared to the original scheme.

III. MODELING OUR ENTANGLEMENT SOURCES

We now describe our realistic model for the ESR-assisted DIQKD scheme discussed above that includes imperfections. All detectors are modeled as on-off photodetectors, i.e., they simply distinguish between vacuum and not vacuum. The model takes into account dark count probability and non-unit efficiency (see Appendix for more details). The sources of polarization entanglement are modeled using realistic SPDCs. A detailed account of the same is described below.

A. Polarization entanglement based on a pair of SPDC sources

Polarization entangled photon pairs form a natural choice for entangled qubits in photonic implementations of QKD. For example, one could consider generating a photon-pair state of the form

$$\propto \left(|H_A, V_B\rangle + |V_A, H_B\rangle\right), \tag{4}$$

where the polarization of the photons that Alice and Bob receive are oppositely correlated.

One way to achieve such an entangled state in practice is to use SPDCs. In particular, we consider the Sagnac loop architecture which uses two down-conversions to generate one entangled photon-pair, by weak pumping of an SPDC crystal from two opposite directions. Because of its configuration, especially the collinear generation of photon-pairs, the Sagnac loop has practical advantages in its compactness, stability, and high brightness (see for example [31] and references therein) compared to the other architectures with single pumping of the crystal. The Sagnac loop architecture was originally invented in [32] and now widely used in recent photonic quantum information processing experiments [23, 33–35]. In theory, the double pumping of the crystal is modeled by two SPDC emissions, more precisely two two-mode squeezed vacua, as described below.

Figure 2 (a) illustrates the Sagnac loop configuration where a single nonlinear crystal is pumped simultaneously from both clockwise (CW) and counter-clockwise (CCW) directions. The crystal is assumed to enable Type-II SPDC, meaning it produces downconverted light in two orthogonal polarization modes. The resulting state can be described as follows. Let us denote the input modes to the Sagnac loop as modes $\hat{a}$ and $\hat{b}$. Then, the state at the output of the two SPDC processes (CW and CCW) can be approximated as $|\Psi\rangle$

$$\begin{aligned} &= \left(c_0 |00\rangle_{a_H a_V} + c_1 |11\rangle_{a_H a_V}\right)\left(c_0 |00\rangle_{b_H b_V} + c_1 |11\rangle_{b_H b_V}\right) \\ &= c_0^2 |0000\rangle_{a_H a_V b_H b_V} + c_1^2 |1111\rangle_{a_H a_V b_H b_V} \\ &+ c_0 c_1 \left(|0011\rangle_{a_H a_V b_H b_V} + |1100\rangle_{a_H a_V b_H b_V}\right), \end{aligned} \tag{5}$$

where we assume $|c_0|^2 + |c_1|^2 \approx 1$ and $|c_1| \ll 1$ and a_H, a_V denote the horizontal and vertical polarization modes in the spatial mode $\hat{a}$, for example.

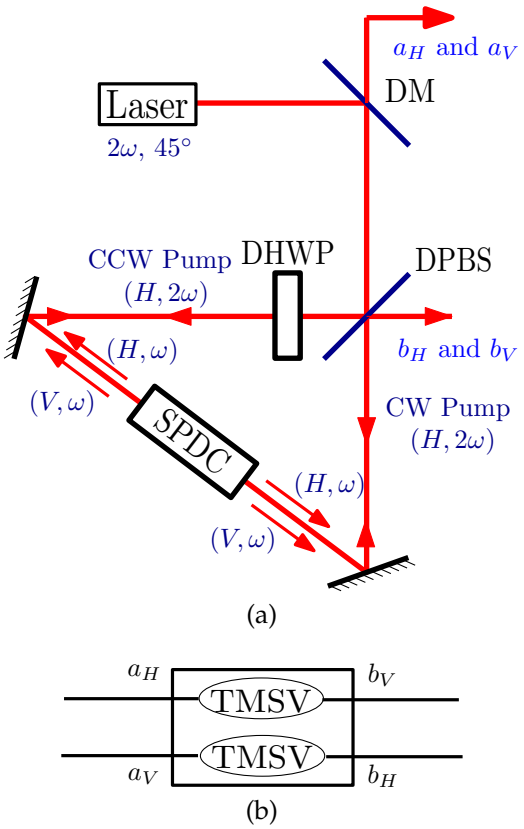

FIG. 2: (a) A Sagnac loop source for generating polarization entanglement based on Type-II SPDC, meaning it produces downconverted light in two orthogonal polarization modes. The SPDC is pumped simultaneously by a clockwise (CW) and a counter-clockwise (CCW) pump. DM stands for a dichroic mirror, which reflects light of frequency 2ω, while being transparent to light of frequency ω. DPBS stands for a dichroic polarizing beamsplitter, which splits light of both frequencies ω and 2ω into its H and V polarization components. DHWP stands for a dichroic halfwave plate at an angle 45°, so that it flips the polarization in the H, V basis as $H \to V$ and $V \to H$. The geometry of the source makes sure that the pump is perfectly recycled, while the downconverted light is output through the topmost and the rightmost modes. (b) A schematic representation of the source. The CW pump generates squeezing in the modes a_H and b_V, while the CCW pump generates squeezing in the other two modes.

This state, when propagated through the polarizing beamsplitter, results in

$$|\Psi\rangle \xrightarrow{\text{PBS}} c_0^2 |0000\rangle_{a_H a_V b_H b_V} + c_1^2 |1111\rangle_{a_H a_V b_H b_V} + c_0 c_1 \left(|0110\rangle_{a_H a_V b_H b_V} + |1001\rangle_{a_H a_V b_H b_V} \right). \quad (6)$$

When post-selected on its two-photon component, this state gives the desired polarization entangled photon pair [31]. The underlying essence behind the generation of entanglement here is the lack of information as to which of the two pumps resulted in the generation of the downconverted photon pairs. Since the underlying source of the photon pair in the considered scheme is a pair of SPDC processes, the source can be exactly modeled as a tensor product of two-mode squeezed vacuums

$$\exp\left(\xi \hat{a}_H^\dagger \hat{b}_V^\dagger - \xi^* \hat{a}_H \hat{b}_V\right) \exp\left(\xi \hat{a}_V^\dagger \hat{b}_H^\dagger - \xi^* \hat{a}_V \hat{b}_H\right) |0\rangle_{a_H} \otimes |0\rangle_{a_V} \otimes |0\rangle_{b_H} \otimes |0\rangle_{b_V} \quad (7)$$

where, e.g., $\hat{a}_H$ and $\hat{a}_H^\dagger$ are the annihilation and creation operators of the mode a_H. Figure 2 (b) depicts this representation of the state produced by the source.

B. Multimode spectral structure of the SPDC outputs

When the parametric down conversion source is pumped by a pulsed laser, the quantum state emitted has a spectral structure, and can be described by [36],

$$\exp\left[\xi \iint d\omega_s d\omega_i f(\omega_s, \omega_i) \hat{a}_s^\dagger(\omega_s) \hat{a}_i^\dagger(\omega_i) - h.c.\right] |0\rangle, \quad (8)$$

where $\xi = r \exp(i\theta)$ is the squeezing parameter (related to the pump power), $\hat{a}_s^\dagger(\omega_s)$ and $\hat{a}_i^\dagger(\omega_i)$ are creation operators for the signal and idler modes with frequencies ω_s and ω_i, respectively. Let us call the above state $|\Psi\rangle$. $f(\omega_s, \omega_i)$ is the joint spectral amplitude, which is a product of the pump distribution and the phase-matching function of the nonlinear crystal [36–38]. We can assume ξ to be real and positive without losing generality.

This joint spectral amplitude can be decomposed using Schmidt decomposition as [37, 38]

$$f(\omega_s, \omega_i) = \sum_l \sqrt{\lambda_l} g_l(\omega_s) h_l(\omega_i), \quad (9)$$

where λ_l, $g_l(\omega_s)$, $h_l(\omega_i)$ are solutions of the eigenvalue equations:

$$\int K_1(\omega, \omega') g_l(\omega') = \lambda_l g_l(\omega'), \quad (10)$$

$$\int K_2(\omega, \omega') h_l(\omega') = \lambda_l h_l(\omega'), \quad (11)$$

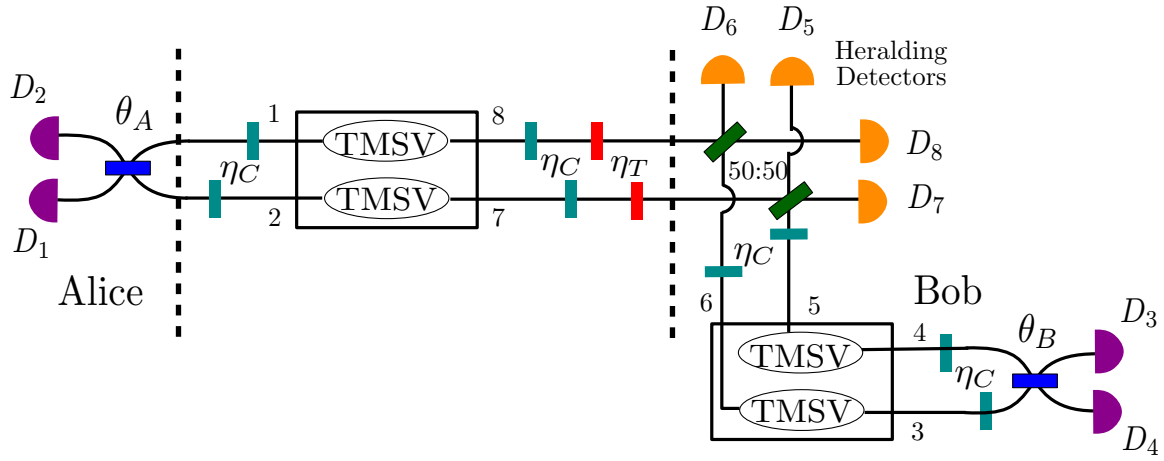

FIG. 3: The ESR-assisted Bell testing setup for DIQKD in greater detail. The Type-II SPDC crystal placed in a Sagnac configuration as depicted in Fig. 2 is used to generate a pair of two-mode squeezed vacuua (TMSV) over polarization modes. The polarizer angle settings at Alice and Bob are denotes as θ_A and θ_B, respectively. The detectors are assumed to be imperfect, on-off photodetectors, with non-unit efficiencies and non-zero dark-count probabilities.

and

$$K_1(\omega,\omega') \equiv \int d\omega_2 f(\omega,\omega_2) f^*(\omega',\omega_2), \quad (12)$$

$$K_2(\omega,\omega') \equiv \int d\omega_1 f(\omega_1,\omega) f^*(\omega_1,\omega'). \quad (13)$$

Then the state in (8) can be represented as

$$|\Psi\rangle = \exp\left[r\sum_l \sqrt{\lambda_l}\hat{b}_l^\dagger \hat{c}_l^\dagger - h.c.\right]|0\rangle \quad (14)$$

$$= \prod_l \exp\left[r\sqrt{\lambda_l}\hat{b}_l^\dagger \hat{c}_l^\dagger - h.c.\right]|0\rangle \quad (15)$$

$$= |\Psi(r\sqrt{\lambda_1})\rangle|\Psi(r\sqrt{\lambda_2})\rangle\cdots, \quad (16)$$

where

$$\hat{b}_l^\dagger = \int d\omega_s g_l(\omega_s)\hat{a}_s^\dagger(\omega_s), \quad (17)$$

$$\hat{c}_l^\dagger = \int d\omega_i h_l(\omega_i)\hat{a}_i^\dagger(\omega_i), \quad (18)$$

and λ_l is the Schmidt eigenvalue. Note that $\hat{b}_l$ and $\hat{c}_l$ satisfy a standard bosonic commutation relation $[\hat{b}_l, \hat{b}_m^\dagger] = [\hat{c}_l, \hat{c}_m^\dagger] = \delta_{lm}$. The decomposition of the exponential term as given in (15) is possible since the Schmidt modes are orthonormal. Finally, (16) represents that in the Schmidt mode basis, the state is described by tensor products of two-mode squeezed vacuums $|\Psi(r\sqrt{\lambda_l})\rangle$, where

$$|\Psi(r\sqrt{\lambda_l})\rangle = \frac{1}{\cosh r\sqrt{\lambda_l}}\sum_n \left(\tanh r\sqrt{\lambda_l}\right)^n |n\rangle_{B_l}|n\rangle_{C_l}, \quad (19)$$

with the effective squeezing parameter $r\sqrt{\lambda_l}$. As a consequence, we conclude that the quantum state emitted from the SPDC source is simply given by a tensor product of two-mode squeezed vacuums. Thus, in the Sagnac loop source-based described previously, when the pump is a pulsed laser, the state in (7) is further a tensor product of TMSVs over appropriate Schmidt modes.

Connection between r and the experimentally observable parameter is the following. Note that the theoretical modeling of $f(\omega_s,\omega_i)$ is well established and thus one can derive the Schmidt eigenvalues for a given setup of the SPDC source. In the experiment, one can also estimate the photon-pair generation rate of the SPDC source, i.e. the probability that the source emits non-zero photons:

$$p = 1 - \prod_l \left|\langle 00|\Psi(r\sqrt{\lambda_l})\rangle\right|^2. \quad (20)$$

Plugging (19) into, (20), we obtain the relation

$$p = 1 - \prod_l \left(\cosh r\sqrt{\lambda_l}\right)^{-2}, \quad (21)$$

which allows us to derive r numerically from experimentally estimated p.

With the above observation and the recent theoretical method developed in [39], one can, e.g., simulate the four-photon HOM experiment including experimental imperfections, infinitely higher order multi-photon components, and joint spectral property of the SPDC source.

IV. RESULTS

Having described our realistic models for the source and the detectors, we now analyze the performance of the ESR-assisted DIQKD scheme with realistic elements. We do so using the characteristic function-based approach from Gaussian quantum information (see the appendix and [39] for more details on the tools we use to perform our calculations). The approach is quite effective to describe and analyze the system consisting of Gaussian elements and on-off photodetectors, taking into account multi-mode structure in the sources, and losses and dark counts in the detectors.

Consider the full, linear optics-based depiction of the ESR-assisted scheme for DIQKD shown in Fig. 3. In this Figure, for simplicity the modes are renumbered 1 through 8, with the odd-numbered modes denoting horizontally polarized modes and the even-numbered modes being vertically polarized. They are generated by SPDC as described in Section III A with the pairs 1 and 8, 2 and 7, etc., being in the two-mode squeezed vacuum state. The polarizers are replaced by beamsplitters between the horizontal/vertical mode pairs, with the tunable transmittivities $\cos^2\theta_A$ and $\cos^2\theta_B$ denoting the polarizer settings. The detectors are assumed to be imperfect, on-off photodetectors, with non-unit efficiencies and non-zero dark-count probabilities.

Firstly, we recall the results presented in [21], where Bob employs the ESR node, but with the detectors modeled as PNRDs. A conclusive detection event in this case refers to the presence of exactly a single photon in the mode. Hence a conclusive-conclusive event at Alice and Bob corresponds to the presence of a maximally entangled photon pair with an intrinsic S value of $2\sqrt{2}$. Any other combination of events at Alice and Bob corresponds to the classical value of $S = 2$. So, the maximal possible violation could be written as the linear combination $S = \mu_{cc} 2\sqrt{2} + (1 - \mu_{cc})\, 2$, where μ_{cc} is the probability of obtaining a conclusive-conclusive event at Alice and Bob. This, when evaluated in the limit of small average photon numbers in the source, resulted in $S \approx 1 + \sqrt{2}$, a constant independent of the distance of transmission.

On the contrary, in our case where we consider on-off photodetectors, a conclusive-conclusive event does not necessarily imply the presence of a maximally entangled photon pair. Thus, we cannot adopt the analysis of [21] and are forced to resort to numerical optimization to determine S values for the state under different conditions of the sources and the detectors. We globally optimize S over the measurement settings at Alice and Bob and the mean photon numbers of the SPDC outputs at the two sources (one being the primary source and the other at the relay node). We use a simulated annealing-based numerical optimization algorithm. We find that the optimal measurement angles at Alice and Bob for the considered loophole-free Bell test are given by $\{0, \pi/6\}$ and $\{\pi/2, 2\pi/3\}$ for the two parties, respectively, and are independent of all other conditions. Assuming symmetric losses in orthogonal polarization modes, we further optimize over an absolute mean photon number, the ratio between the mean photon numbers of the primary source and the source in the relay node, and the ratio between the mean photon numbers of the two SPDC within a source.

We present our results in two parts. Firstly, we focus on the potential S value of the state heralded upon successful entanglement swapping as a function of the communication distance assuming a telecommunication fiber of attenuation $\alpha = 0.2$ dB/km. Here, we assume ideal coupling and detectors at the end users Alice and Bob, but real, imperfect ones at the relay node. Secondly, we consider real, imperfect coupling and detectors all over including at Alice and Bob and analyze the S value as a function of distance. Here, we also separately optimize K to evaluate the performance of the scheme for key distribution. We assume that the sources have a single pure Schmidt mode by default unless mentioned otherwise. In the latter cases, we assume that there are predominantly two Schmidt modes and we denote the leading Schmidt eigenvalue as λ, with the other being $1 - \lambda$.

A. With ideal coupling and detectors at Alice and Bob, but real ones at the relay node

Assuming ideal detectors at Alice and Bob, we find that the S value for the heralded state is constant over distance and is independent of the efficiency of the heralding detectors (Fig. 4 (a)). Although the value of S is less than the maximum violation at zero distance obtainable in the absence of the ESR (see black curve in Fig. 4), the fact that

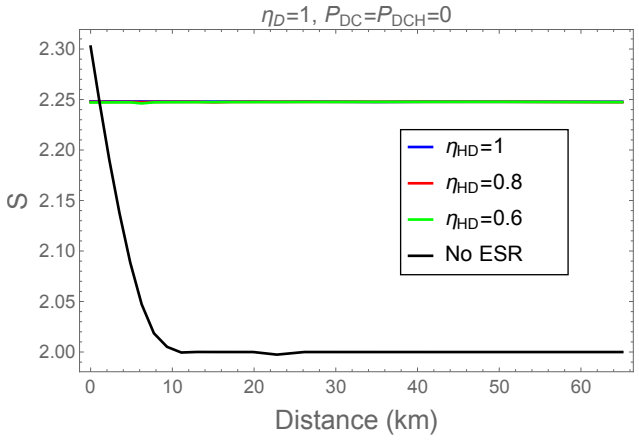

(a)

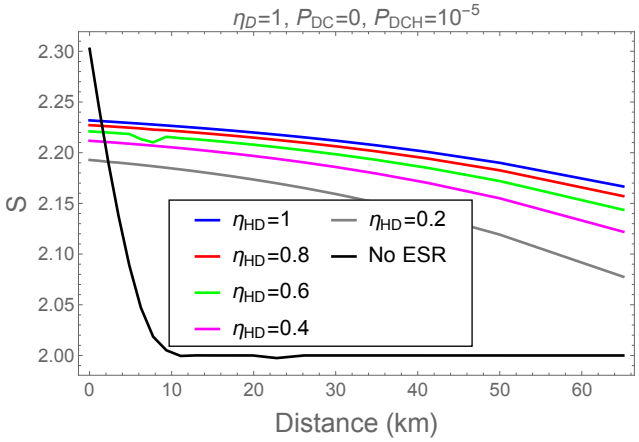

(b)

FIG. 4: (Color online) Maximal loophole-free violation of the CHSH inequality S as a function of distance in the ESR-assisted DIQKD of Fig. 3. The sources are assumed to be monochromatic. The detection efficiencies at Alice and Bob are assumed to be ideal (i.e., the product of coupling and detector efficiencies $\eta_D = \eta_C\eta_{\rm det} = 1$ and dark count probability in the detectors $P_{DC} = 0$). The quantities $\eta_{HD} = \eta_C\eta_{\rm hdet}$ and P_{DCH} denote the detection efficiency and dark count probability, respectively, for the heralding modes / detectors. Curves corresponding to various values of η_{HD} are plotted for the cases (a) without ($P_{DCH} = 0$) and (b) with dark counts ($P_{DCH} \neq 0$) in the heralding detectors. The common reference (black) curve in both (a) and (b) corresponds to the case where the ESR node is absent. In (a), the S curves coincide, while in (b), from top (blue) to bottom (gray), the curves correspond to decreasing values of η_{HD}.

it is independent of distance in principle is interesting. As explained previously, this feature was also observed in [21], where PNRDs were employed. On the other hand, when heralding detectors with a dark count probability $P_{DCH} = 10^{-5}$ are used, the

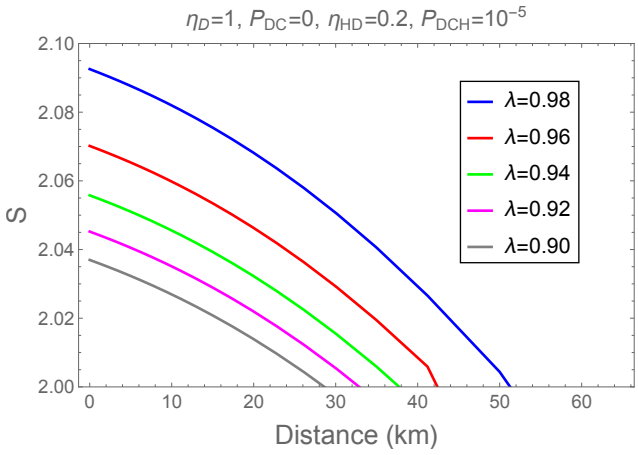

FIG. 5: (Color online) Maximal loophole-free violation S as a function of distance for different spectral spreads in the sources for the ESR-assisted DIQKD scheme. λ here denotes the largest Schmidt eigenvalue in the Schmidt decomposition of the joint spectral density. The curves from top (blue) to bottom (gray) correspond to decreasing values of λ. The detection efficiencies at Alice and Bob are assumed to be ideal (i.e., the product of coupling and detector efficiencies $\eta_D = \eta_C\eta_{\rm det} = 1$ and dark count probability in the detectors $P_{DC} = 0$), while the detection efficiencies in the heralding modes are taken as $\eta_{HD} = 0.2$ and the dark count probability in the heralding detectors as $P_{DCH} = 10^{-5}$.

constancy of S no longer holds. Nevertheless, its value is still significantly higher than the case without the relay node for considerably larger range of distances (Fig. 4 (b)).

Next, we include spectral spread in the sources, namely the multimode nature $\lambda < 1$. The detector efficiencies are assumed to be flat over all the spectral modes. In Fig. 5, we plot S vs distance for various values of λ for the case of a realistic heralding detection efficiency of $\eta_{HD} = 0.2$ and dark count probability $P_{DC} = 10^{-5}$. We find that S values drops to the classical value of 2 faster with increasing spectral impurity. The real cause for the faster degradation of S vs distance with increasing spectral impurity in the sources is that the on-off detectors cannot discriminate clicks from different spectral modes, which destroy the entanglement correlation in each mode. Thus, if a Schmidt mode separator were possible to implement in front of the detector set, there might be no degradation, but mode multiplexed performance instead. Unfortunately such a separator is not easy to realize. Nevertheless, the largest distance at which $S > 2$ even for $\lambda = 0.95$ is about 30kms, which is still larger compared to the 10km

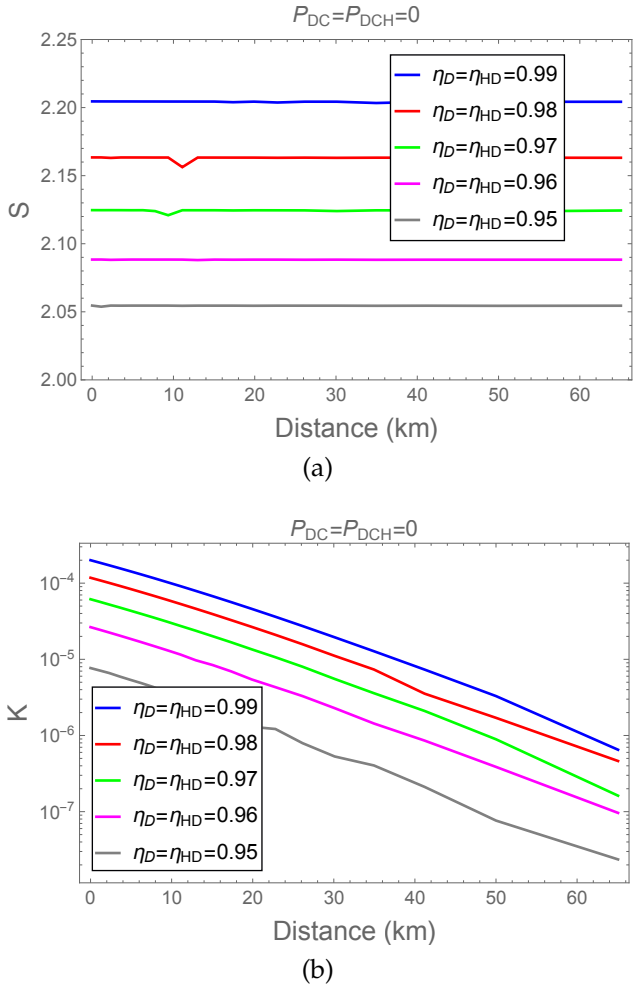

FIG. 6: (Color online) (a) Maximal loophole-free violation of the CHSH inequality S and (b) a lower bound on the key rate K (bits per channel use), as a function of distance. The sources are assumed to be monochromatic. All detection efficiencies are assumed to be of non-unity (η_D and η_{HD} denoting the detection efficiencies at the end users, and the heralding detectors, respectively), but free from dark count ($P_{DC} = P_{DCH} = 0$). The curves from top (blue) to bottom (gray) correspond to decreasing values of detection efficiencies $\eta_D = \eta_{HD} = \eta$.

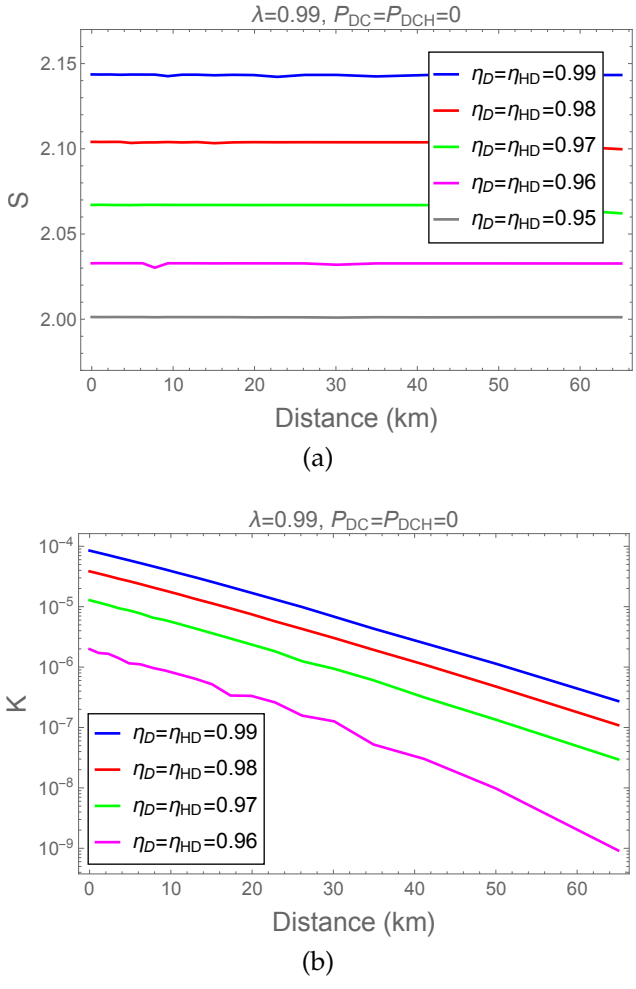

FIG. 7: (Color online) Effect of spectral impurity (where the leading Schmidt eigenvalue λ is 0.99) in the sources. (a) The maximal loophole-free violation of the CHSH inequality S and (b) a lower bound on the key rate, K (bits per channel use), are plotted as a function of distance. All detection efficiencies are assumed to be of non-unity (η_D and η_{HD} denoting the detection efficiencies at the end users, and the heralding detectors, respectively), but free from dark count ($P_{DC} = P_{DCH} = 0$). The curves from top (blue) to bottom (gray in (a) and pink in (b)) correspond to decreasing values of detection efficiencies $\eta_D = \eta_{HD} = \eta$.

limit at which S drops to 2 in the absence of the ESR node.

B. With real, imperfect coupling and detectors all over

Assuming identical, imperfect detectors at both Alice and Bob as well as at the ESR, we now analyze the S and K values as functions of distance. In the absence of dark counts in the detectors, we once again find S to be independent of the distance, but to decrease towards the classical value of 2 with decreasing values of the detection efficiencies $\eta_D = \eta_{HD}$ (Fig. 6 (a)). The key rate K similarly monotonically decreases with the detection inefficiencies while keeping an exponential behavior in the drop with respect to distance (Fig. 6 (b)). We now briefly compare the K values of Fig. 6 (b) with those reported in [21]. The calculations employed in the two are identical, but the results are marginally different, because we use on-off pho-

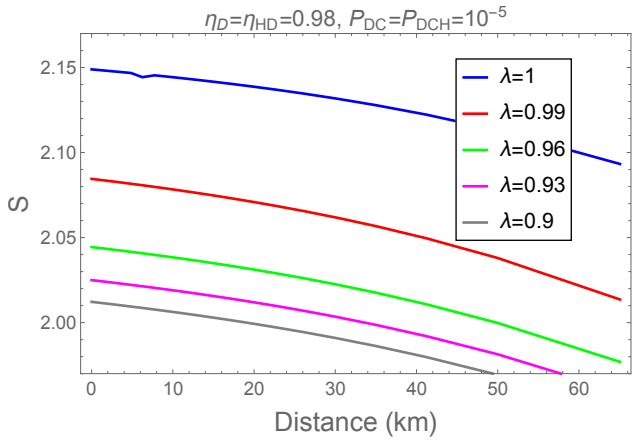

(a)

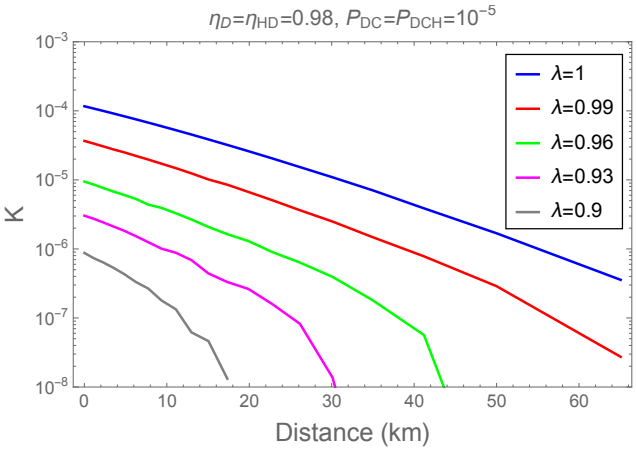

(b)

FIG. 8: (Color online) Variation due to the multimode spectral structure in the sources. (a) The maximal loophole-free violation of the CHSH inequality S and (b) a lower bound on the key rate, K (bits per channel use), are plotted as a function of distance. All detection efficiencies are assumed to be non-unity ($\eta_D = \eta_{HD} = 0.98$, where η_D and η_{HD} denote the detection efficiencies at the end users, and the heralding detectors, respectively) and dark count probability $P_{\rm DC} = 10^{-5}$. The curves from top (blue) to bottom (gray) correspond to decreasing values of the largest Schmidt eigenvalue λ.

todetector while [21] used PNRDs. The PNRDs enable higher K values at short distances than the on-off detectors, but we find that the performances of the two types of detectors even out at larger distances. For, example, $K \approx 10^{-6}$ bits per channel use at a distance of about 60kms with both types of detectors. In any case, the main point of emphasis here is that rates enabled by the ESR are obviously much higher than what is possible without the relay.

Next, we include spectral imperfections in the sources. The same behavior as above holds, but with diminished values of S and K. Figs. 7 (a) and (b) illustrate the point for sources with a leading Schmidt eigenvalue of $\lambda = 0.99$. Finally, when dark counts are included ($P_{DC} = 10^{-5}$), both S and K drop with distance at faster rates corresponding to decreasing values of λ (Figs. 8 (a) and (b)). The K curves in this case exhibit the familiar cliff-type drop to zero when the dark count rate becomes comparable to the signal rate, which decreases with distance.

V. CONCLUSIONS

We investigated a scheme for DIQKD that is based on the use of a simple, conventional ESR node to mitigate the effect of transmission losses. Going beyond earlier work of Curty and Moroder [21], we considered a more realistic model for the entangled source and the detectors. Our sources of polarization-entanglement were taken to be based on a pair of pulsed SPDCs, having infinitely higher order multi-photon components and multimode spectral structure. Our detectors were taken to be spectrally-flat on-off photodetectors, which simply distinguish the event of presence of photons from absence. The detectors included losses (contributions from detector inefficiency and free-space to fiber coupling inefficiency) and dark counts. We presented an exact key rate analysis for the scheme based on the use of tools from Gaussian quantum information. Our results showed that the relay node enables positive key rates over larger distances than what is possible without the relay node for sufficiently large detection efficiencies (which includes detector and free-space to fiber coupling efficiencies), small dark count probabilities in the detectors and small spectral spread in the sources. Thus, our results established the robustness of the ESR-based scheme for DIQKD against imperfections in the sources and detectors.

While our analyses captured the effects of imperfections in the SPDC sources and in the detection process to a large extent, there is room for further refinement. For example, in the multimode spectral modeling of the sources, more terms in the Schmidt decomposition could be included. In the model for the on-off photodetectors, spectrally-dependent efficiencies could be considered. Since the source is

based on a pulsed laser, temporal mode mismatch could be included in the overall model.

To conclude, our results ascertain that it is possible to mitigate transmission losses using the ESR node with more realistic models for the sources and detectors than what was considered in [21]. However, the ultimate practical realizability of DIQKD still hinges on improvements the detector technologies. As noted in [21] and concurred by our analyses in this paper, detection efficiencies upwards of 95% are required to realize DIQKD even in the case that the source spectral purity is one and the detectors are dark count-free. Recent progress in coupling and detector technologies shows promise that such high detection efficiencies might be achievable in the not-so-distant future.

Acknowledgments

KPS thanks the National Institute of Information and Communications Technologies, Tokyo, for their hospitality during the summer of 2015, when a majority of this work was carried out. KPS acknowledges funding from the National Science Foundation (NSF) under Award No. CCF-1350397 and the Max Planck Society. The authors thank Marcos Curty, Jonathan Dowling, Ruibo-Jin, George Knee, Bill Munro, Kae Nemoto and Mark M. Wilde for valuable discussions. This work was supported from Open Partnership Bilateral Joint Research Projects (JSPS) and ImPACT Program of Council for Science, Technology and Innovation (Cabinet Office, Government of Japan).

[1] V. Scarani, H. Bechmann-Pasquinucci, N. J. Cerf, M. Dušek, N. Lütkenhaus, and M. Peev, Reviews of Modern Physics **81**, 1301 (2009), arXiv:0802.4155, URL http://link.aps.org/doi/10.1103/RevModPhys.81.1301.

[2] N. Gisin, G. Ribordy, W. Tittel, and H. Zbinden, Rev. Mod. Phys. **74**, 145 (2002), URL http://link.aps.org/doi/10.1103/RevModPhys.74.145.

[3] C. H. Bennett and G. Brassard, in *Proceedings of IEEE International Conference on Computers Systems and Signal Processing* (Bangalore, India, 1984), pp. 175–179.

[4] A. K. Ekert, Phys. Rev. Lett. **67**, 661 (1991), URL http://link.aps.org/doi/10.1103/PhysRevLett.67.661.

[5] C. H. Bennett, Phys. Rev. Lett. **68**, 3121 (1992), URL http://link.aps.org/doi/10.1103/PhysRevLett.68.3121.

[6] F. Grosshans and P. Grangier, Phys. Rev. Lett. **88**, 057902 (2002), URL http://link.aps.org/doi/10.1103/PhysRevLett.88.057902.

[7] V. Scarani, A. Acín, G. Ribordy, and N. Gisin, Phys. Rev. Lett. **92**, 057901 (2004), URL http://link.aps.org/doi/10.1103/PhysRevLett.92.057901.

[8] H.-K. Lo, X. Ma, and K. Chen, Phys. Rev. Lett. **94**, 230504 (2005), URL http://link.aps.org/doi/10.1103/PhysRevLett.94.230504.

[9] D. Mayers and A. Yao, in *Proceedings of the 39th Annual Symposium on Foundations of Computer Science* (IEEE Computer Society, Washington, DC, USA, 1998), FOCS '98, pp. 503–, ISBN 0-8186-9172-7, URL http://dl.acm.org/citation.cfm?id=795664.796390.

[10] U. Vazirani and T. Vidick, Phys. Rev. Lett. **113**, 140501 (2014), URL http://link.aps.org/doi/10.1103/PhysRevLett.113.140501.

[11] S. Pironio, A. Acin, N. Brunner, N. Gisin, S. Massar, and V. Scarani, New Journal of Physics **11**, 045021 (2009), URL http://stacks.iop.org/1367-2630/11/i=4/a=045021.

[12] A. Acin, N. Brunner, N. Gisin, S. Massar, S. Pironio, and V. Scarani, Phys. Rev. Lett. **98**, 230501 (2007), URL http://link.aps.org/doi/10.1103/PhysRevLett.98.230501.

[13] N. Brunner, D. Cavalcanti, S. Pironio, V. Scarani, and S. Wehner, Rev. Mod. Phys. **86**, 419 (2014), URL http://link.aps.org/doi/10.1103/RevModPhys.86.419.

[14] B. Hensen, H. Bernien, A. E. Dreau, A. Reiserer, N. Kalb, M. S. Blok, J. Ruitenberg, R. F. L. Vermeulen, R. N. Schouten, C. Abellan, et al., Nature **advance online publication** (2015), ISSN 1476-4687, URL http://dx.doi.org/10.1038/nature1575910.1038/nature15759http://www.nature.com/nature/journal/vaop/ncurrent/abs/nature15759.html#supplementary-information.

[15] M. Giustina, M. A. M. Versteegh, S. Wengerowsky,

J. Handsteiner, A. Hochrainer, K. Phelan, F. Steinlechner, J. Kofler, J.-A. Larsson, C. Abellan, et al., *A significant-loophole-free test of Bell's theorem with entangled photons* (2015), arXiv:1511.03190v1, 1511.03190.

[16] L. K. Shalm, E. Meyer-Scott, B. G. Christensen, P. Bierhorst, M. A. Wayne, M. J. Stevens, T. Gerrits, S. Glancy, D. R. Hamel, M. S. Allman, et al., *A strong loophole-free test of local realism* (2015), arXiv:1511.03189v1, 1511.03189.

[17] T. C. Ralph and A. P. Lund, AIP Conference Proceedings **1110**, 155 (2009), URL http://scitation.aip.org/content/aip/proceeding/aipcp/10.1063/1.3131295.

[18] N. Gisin, S. Pironio, and N. Sangouard, Phys. Rev. Lett. **105**, 070501 (2010), URL http://link.aps.org/doi/10.1103/PhysRevLett.105.070501.

[19] A. I. Lvovsky, Nat Phys **9**, 5 (2013), ISSN 1745-2473, URL http://dx.doi.org/10.1038/nphys2517.

[20] S. Kocsis, G. Y. Xiang, T. C. Ralph, and G. J. Pryde, Nat Phys **9**, 23 (2013), ISSN 1745-2473, URL http://dx.doi.org/10.1038/nphys2469.

[21] M. Curty and T. Moroder, Phys. Rev. A **84**, 010304 (2011), URL http://link.aps.org/doi/10.1103/PhysRevA.84.010304.

[22] J. F. Clauser, M. A. Horne, A. Shimony, and R. A. Holt, Phys. Rev. Lett. **23**, 880 (1969), URL http://link.aps.org/doi/10.1103/PhysRevLett.23.880.

[23] R.-B. Jin, M. Takeoka, U. Takagi, R. Shimizu, and M. Sasaki, Scientific Reports **5**, 9333 (2015), URL http://dx.doi.org/10.1038/srep0933310.1038/srep09333.

[24] M. Halder, A. Beveratos, N. Gisin, V. Scarani, C. Simon, and H. Zbinden, Nat Phys **3**, 692 (2007), ISSN 1745-2473, URL http://dx.doi.org/10.1038/nphys700.

[25] J.-W. Pan, D. Bouwmeester, H. Weinfurter, and A. Zeilinger, Phys. Rev. Lett. **80**, 3891 (1998), URL http://link.aps.org/doi/10.1103/PhysRevLett.80.3891.

[26] C. C. W. Lim, C. Portmann, M. Tomamichel, R. Renner, and N. Gisin, Phys. Rev. X **3**, 031006 (2013), URL http://link.aps.org/doi/10.1103/PhysRevX.3.031006.

[27] A. Acin, S. Massar, and S. Pironio, New Journal of Physics **8**, 126 (2006), URL http://stacks.iop.org/1367-2630/8/i=8/a=126.

[28] B. Cirel'son, Letters in Mathematical Physics **4**, 93 (1980), ISSN 0377-9017, URL http://dx.doi.org/10.1007/BF00417500.

[29] I. Devetak and A. Winter, Proceedings of the Royal Society of London A: Mathematical, Physical and Engineering Sciences **461**, 207 (2005), ISSN 1364-5021.

[30] V. Caprara Vivoli, P. Sekatski, J.-D. Bancal, C. C. W. Lim, B. G. Christensen, A. Martin, R. T. Thew, H. Zbinden, N. Gisin, and N. Sangouard, Phys. Rev. A **91**, 012107 (2015), URL http://link.aps.org/doi/10.1103/PhysRevA.91.012107.

[31] R.-B. Jin, R. Shimizu, K. Wakui, M. Fujiwara, T. Yamashita, S. Miki, H. Terai, Z. Wang, and M. Sasaki, Opt. Express **22**, 11498 (2014), URL http://www.opticsexpress.org/abstract.cfm?URI=oe-22-10-11498.

[32] B. S. Shi and A. Tomita, Physical Review A **69**, 013803 (2004).

[33] R. Prevedel, D. R. Hamel, R. Colbeck, K. Fisher, and K. J. Resch, Nat. Phys. **7**, 757761 (2011).

[34] M. Giustina, A. Mech, S. Ramelow, B. Wittmann, J. Kofler, J. Beyer, A. Lita, B. Calkins, T. Gerrits, S. W. Nam, et al., Nature **497**, 227 (2013), ISSN 0028-0836, URL http://dx.doi.org/10.1038/nature1201210.1038/nature12012.

[35] Y. Cao, H. Liang, J. Yin, H. L. Yong, F. Zhou, Y. P. Wu, J. G. Ren, Y. H. Li, G. S. Pan, X. Yang, T. Ma, et al., Opt. Express **21**, 27260 (2013).

[36] W. P. Grice and I. A. Walmsley, Physical Review A **56**, 1627 (1997), ISSN 1050-2947.

[37] C. K. Law, I. A. Walmsley, and J. H. Eberly, Physical Review Letters **84**, 5304 (2000), ISSN 0031-9007.

[38] P. J. Mosley, J. S. Lundeen, B. J. Smith, P. Wasylczyk, A. B. U'Ren, C. Silberhorn, and I. a. Walmsley, Physical Review Letters **100**, 1 (2008), ISSN 00319007, 0711.1054.

[39] M. Takeoka, R.-b. Jin, and M. Sasaki, New Journal of Physics **17**, 43030 (2015), ISSN 1367-2630, URL http://dx.doi.org/10.1088/1367-2630/17/4/043030.

[40] G. Adesso, S. Ragy, and A. R. Lee, Open Systems & amp; Information Dynamics **21**, 1440001 (2014).

[41] C. Weedbrook, S. Pirandola, R. Garcia-Patron, N. J. Cerf, T. C. Ralph, J. H. Shapiro, and S. Lloyd, Reviews of Modern Physics **84**, 621 (2012), arXiv:1110.3234.

Appendix: The Characteristic Function Approach to Photonic Quantum information processing

In continuous-variable quantum information processing, there exist powerful tools based on the characteristic functions of quantum states, which are particularly useful when dealing with Gaussian states and Gaussian operations [40, 41]. Since entangled photon pairs, in practice, are post-selected from continuous-variable sources such as SPDCs, these tools lend themselves rather naturally for an easy and exact treatment of photonic quantum information processing tasks (cf. [39]) without the need for any approximations. Here we present a

brief review of these tools for the convenience of the reader. (For a more comprehensive review, see [40, 41].)

Consider N Bosonic modes associated with a tensor product Hilbert space $\mathcal{H}^{\otimes N} = \otimes_{j=1}^{N} \mathcal{H}_j$, where each $\mathcal{H}_j$ is an infinite-dimensional Hilbert space. Corresponding to each mode is a pair of field operators $\hat{a}_j$ and $\hat{a}_j^\dagger$–the annihilation and creation operators–which satisfy the canonical commutation relation given by

$$\left[\hat{a}_j, \hat{a}_k^\dagger\right] = \delta_{jk}. \tag{22}$$

It is common to define the quadrature operators of a bosonic mode as

$$\hat{x}_j = \frac{1}{\sqrt{2}}\left(\hat{a}_j + \hat{a}_j^\dagger\right), \tag{23}$$

$$\hat{p}_j = \frac{1}{\sqrt{2}i}\left(\hat{a}_j - \hat{a}_j^\dagger\right), \tag{24}$$

where these operators can be verified to obey the commutation relation

$$\left[\hat{x}_j, \hat{p}_k\right] = i\delta_{jk}. \tag{25}$$

(Note that we choose as a convention $\hbar = 1$.)

Let $\hat{\rho}$ be a density operator defined on $\mathcal{H}^{\otimes N}$, which represents a quantum state in the N-mode Hilbert space. The characteristic function of $\hat{\rho}$ is defined to be

$$\chi(\xi) = \mathrm{Tr}\left\{\hat{\rho}\hat{\mathcal{W}}(\xi)\right\}, \tag{26}$$

where

$$\hat{\mathcal{W}}(\xi) = \exp\left(-i\xi^T\hat{R}\right) \tag{27}$$

is known as the Weyl operator, and

$$\hat{R} = [\hat{x}_1, \ldots \hat{x}_N, \hat{p}_1, \ldots \hat{p}_N], \tag{28}$$

$$\xi = [\xi_1, \ldots, \xi_{2N}],\ \xi_i \in \mathbb{R} \forall i. \tag{29}$$

A. Gaussian States

A Gaussian state is a quantum state whose characteristic function is Gaussian, i.e., of the form:

$$\chi(x) = \exp\left[-\frac{1}{4}x^{\mathrm{T}}\gamma x - i\,\mathrm{d}^{\mathrm{T}}x\right], \tag{30}$$

where γ is a $2n \times 2n$ matrix called the covariance matrix and d is a $2n$-dimensional vector known as the displacement vector. The simplest example of a Gaussian state is the coherent state

$$|\alpha\rangle = \exp\left(\alpha a^\dagger - \alpha^* a\right)|0\rangle,\ \alpha = |\alpha|\exp\left(i\phi\right), \tag{31}$$

$$= \exp\left(-\frac{|\alpha|^2}{2}\right)\sum_{n=0}^{\infty}\frac{\alpha^n}{\sqrt{n!}}|n\rangle. \tag{32}$$

Its covariance matrix is the 2×2 identity matrix, and displacement vector is

$$\alpha = \sqrt{2}\begin{pmatrix}\mathrm{Re}(\alpha)\\ \mathrm{Im}(\alpha)\end{pmatrix}. \tag{33}$$

Another common example of a Gaussian state is the two-mode squeezed vacuum state, which is generated by an SPDC source

$$|\xi\rangle = \exp\left(\xi a^\dagger b^\dagger - \xi^* ab\right)|0\rangle_a \otimes |0\rangle_b \tag{34}$$

$$= \frac{1}{\cosh r}\sum_{n=0}^{\infty}\left(\exp(i\theta)\tanh r\right)^n |n\rangle_a \otimes |n\rangle_b, \tag{35}$$

where $\xi = r\exp(i\theta)$ is the squeezing parameter. The TMSV has zero displacement and a covariance matrix given by

$$\gamma^{\mathrm{TMSV}}(\mu) = \begin{pmatrix}\gamma^+(\mu) & 0\\ 0 & \gamma^-(\mu)\end{pmatrix}, \tag{36}$$

where μ is the average photon number in each mode of the state and

$$\gamma^\pm(\mu) = \begin{pmatrix}2\mu+1 & \pm 2\sqrt{\mu(\mu+1)}\\ \pm 2\sqrt{\mu(\mu+1)} & 2\mu+1\end{pmatrix}. \tag{37}$$

A very convenient property of the characteristic function representation of a multimode Gaussian state is that the reduced state on any subsystem is simply given by the corresponding sub-matrix of the displacement vector and the covariance matrix of the full state. For example, consider the TMSV. The reduced state on any one of the two modes is a thermal state

$$\rho^{\mathrm{th}} = \sum_{n=0}^{\infty}\frac{\mu^n}{(\mu+1)^{n+1}}|n\rangle\langle n|, \tag{38}$$

whose covariance matrix is given by

$$\gamma^{\mathrm{th}} = \begin{pmatrix}2\mu+1 & 0\\ 0 & 2\mu+1\end{pmatrix}, \tag{39}$$

which is precisely what the corresponding sub-matrix of γ^{TMSV} is.

B. Gaussian operations

By a quantum operation, we mean a linear map $\mathcal{E} : \rho \to \mathcal{E}(\rho)$ (where ρ is a quantum state, i.e., $\rho \geq 0$ and $\mathrm{Tr}(\rho) = 1$)), which is completely positive, i.e. $(\mathrm{id} \otimes \mathcal{E})(\sigma \otimes \rho)$ is also a valid quantum state for all positive operators σ, and trace reducing, i.e., $0 \leq \mathrm{Tr}(\mathcal{E}(\rho)) \leq 1$. A quantum operation is called a quantum channel if it is trace preservation, i.e., $\mathrm{Tr}(\mathcal{E}(\rho)) = 1$. Further, the special case of quantum channels that are reversible are the unitary transformations $U^{-1} = U^{\dagger}$, which transform a quantum state ρ as $\rho \to U\rho U^{\dagger}$.

A quantum operation is called a Gaussian operation if it maps Gaussian states to Gaussian states. Also likewise, Gaussian unitaries are defined to be unitaries that map Gaussian states to Gaussian states. The action of a Gaussian unitary U on a state ρ can be easily described easily by a corresponding real symplectic transformation S on the covariance matrix γ and the displacement vector d of the state

$$\gamma \to S^{\mathrm{T}} \gamma S, \; \mathrm{d} \to S^{\mathrm{T}} \mathrm{d}\,. \tag{40}$$

The symplectic transformation corresponding to a simple phase shift unitary on a single mode is given by

$$R\left(\phi\right) = \begin{pmatrix} \cos\phi & \sin\phi \\ -\sin\phi & \cos\phi \end{pmatrix}. \tag{41}$$

Likewise, that corresponding to a beamsplitter of transmittivity t between two modes is given by

$$S\left(t\right) = \begin{pmatrix} \sqrt{t} & \sqrt{1-t} & 0 & 0 \\ -\sqrt{1-t} & \sqrt{t} & 0 & 0 \\ 0 & 0 & \sqrt{t} & \sqrt{1-t} \\ 0 & 0 & -\sqrt{1-t} & \sqrt{t} \end{pmatrix}. \tag{42}$$

C. Photodetectors

We consider on-off photodetectors, meaning that the detectors simply distinguish between vacuum and not vacuum. These detectors can be represented as the following positive operator valued measure (POVM):

$$\begin{aligned} \Pi_0 &= |0\rangle\langle 0|\,, \\ \Pi_1 &= \sum_{n=1}^{\infty} |n\rangle\langle n| = I - \Pi_0. \end{aligned} \tag{43}$$

When a single-mode Gaussian state ρ with characteristic function $\chi_\rho(x) = \exp\left(-\frac{1}{4}x^{\mathrm{T}}\gamma x\right)$ is measured using a on-off photodetector, the probability of detecting photons ("on" outcome) is given by

$$\begin{aligned} p_1 &= \mathrm{Tr}\left(\rho\Pi_1\right) = 1 - \mathrm{Tr}\left(\rho\Pi_0\right) \\ &= 1 - \frac{1}{2\pi}\int dx\, \chi_\rho(x)\, \chi_{|0\rangle\langle 0|}(-x) \\ &= 1 - \frac{1}{2\pi}\int dx\, \exp\left(-\frac{1}{4}x^{\mathrm{T}}\left(\gamma + I\right)x\right) \\ &= 1 - \frac{2}{\sqrt{\det\left(\gamma + I\right)}}. \end{aligned} \tag{44}$$

Likewise, when an m-mode Gaussian state is measured using on-off photodetectors in all the modes, the probability of coincidence detection ("on" outcome in all the modes) is given by

$$p_{\text{coinc.}} = \sum_{\tau \in \mathcal{P}(\mathcal{K})} (-1)^{|\tau|} \frac{2^{|\tau|}}{\sqrt{\det\left(\gamma^{(\tau)} + I_{|\tau|}\right)}}, \tag{45}$$

where $\mathcal{K}$ is a set consisting of the m modes, $\mathcal{P}(\mathcal{K})$ is the powerset of $\mathcal{K}$–meaning the set of all subsets of $\mathcal{K}$, $\gamma^{(\tau)}$, e.g., is the covariance matrix of the reduced state on the modes in element τ, and $I_{|\tau|}$ is the identity matrix of dimension $|\tau|$.

D. Imperfections in the channel and the detectors

The primary imperfection in the optical channel is photon loss, e.g., losses in transmission and in coupling between media. It is known that the lossy optical channel is a Gaussian channel. And a typical model for the channel is a pure loss bosonic channel, which is a beamsplitter transformation of transmittivity t between the lossy mode and a vacuum mode. The action of the lossy optical channel on the state of a mode with covariance matrix γ can be described as

$$\mathcal{L}^t : \gamma \to K^{\mathrm{T}}\gamma K + \alpha, \tag{46}$$

where $K = \sqrt{t}I$ and $\alpha = (1-t)\,I$.

The imperfections in the on-off photodetectors include (a) photon loss–this is modeled as a lossy channel of the above type followed by a lossless detector, (b) dark counts–these are modeled by amending the detector POVM elements as

$$\Pi_0(\nu) = (1-\nu)\,|0\rangle\langle 0|\,, \tag{47}$$

$$\Pi_1(\nu) = I - \Pi_0(\nu)\,, \tag{48}$$

where ν is the dark count probability.